Boundary-Layer Meteorol (2012) 144:217–241
DOI 10.1007/s10546-012-9719-4

ARTICLE

Shear-Stress Partitioning in Live Plant Canopies and Modifications to Raupach's Model

Benjamin Walter · Christof Gromke · Michael Lehning

Received: 1 November 2011 / Accepted: 13 March 2012 / Published online: 10 April 2012

Abstract The spatial peak surface shear stress τ_S'' on the ground beneath vegetation canopies is responsible for the onset of particle entrainment and its precise and accurate prediction is essential when modelling soil, snow or sand erosion. This study investigates shear-stress partitioning, i.e. the fraction of the total fluid stress on the entire canopy that acts directly on the surface, for live vegetation canopies (plant species: *Lolium perenne*) using measurements in a controlled wind-tunnel environment. Rigid, non-porous wooden blocks instead of the plants were additionally tested for the purpose of comparison since previous wind-tunnel studies used exclusively artificial plant imitations for their experiments on shear-stress partitioning. The drag partitioning model presented by Raupach (Boundary-Layer Meteorol 60:375–395, 1992) and Raupach et al. (J Geophys Res 98:3023–3029, 1993), which allows the prediction of the total shear stress τ on the entire canopy as well as the peak $(\tau_S''/\tau)^{1/2}$ and the average $(\tau_S'/\tau)^{1/2}$ shear-stress ratios, is tested against measurements to determine the model parameters and the model's ability to account for shape differences of various roughness elements. It was found that the constant c, needed to determine the total stress τ and which was unspecified to date, can be assumed a value of about $c = 0.27$. Values for the model parameter m, which accounts for the difference between the spatial surface average τ_S' and the peak τ_S'' shear stress, are difficult to determine because m is a function of the roughness density, the wind velocity and the roughness element shape. A new definition for a parameter a is suggested as a substitute for m. This a parameter is found to be more closely universal and solely a function of the roughness element shape. It is able to predict the peak surface shear stress accurately. Finally, a method is presented to determine the new a parameter for different kinds of roughness elements.

B. Walter (✉) · C. Gromke · M. Lehning
WSL Institute for Snow and Avalanche Research SLF, 7260 Davos Dorf, Switzerland
e-mail: walter@slf.ch

B. Walter · M. Lehning
CRYOS, School of Architecture, Civil and Environmental Engineering,
École Polytechnique Fédéral de Lausanne, Lausanne, Switzerland

Keywords Boundary-layer flow · Drag partitioning · Irwin sensor · Shear-stress ratio · Vegetation canopy · Wind tunnel

List of Symbols

A_f	Roughness element frontal area
A	Effective shelter area
C_R	Roughness element drag coefficient
C_S	Surface drag coefficient
R^2	Coefficient of determination
$Re_h = U_h h/\nu$	Roughness element Reynolds number
S	Total surface area per roughness element
S'	Exposed surface area per roughness element
U_δ	Free stream velocity
$\langle U_i \rangle$	Spatiotemporally-averaged velocity inside the canopy
U_h	Mean velocity at top of roughness elements
V	Effective shelter volume
a	τ_S''/τ_S' peak mean stress ratio
a_i	Fit parameters
b	Roughness element width
b_i	Fit parameters
c, c_i, c' and c''	Constants of proportionality
h	Roughness element height
m	Parameter defining relation between τ_S'' and τ_S'
$u_* = (\tau/\rho)^{1/2}$	Friction velocity
u_τ	Skin friction velocity
$-\overline{u'w'}$	Kinematic Reynolds stress
z_0	Aerodynamic roughness length
$\beta = C_\mathrm{R}/C_\mathrm{S}$	Roughness element to surface drag coefficient ratio
$\lambda = A_f/S$	Roughness density
$\nu \approx 1.5 \times 10^{-5}\,\mathrm{m^2\,s^{-1}}$	Kinematic viscosity of air
Φ	Force on single roughness element
ρ	Air density
σ	Ratio of roughness element basal to frontal area
$\tau = \rho u_*^2$	Total shear stress on entire canopy
τ_R	Shear stress acting on roughness elements
τ_S	Spatial average surface shear stress on area S
$\tau_S\,(x, y)$	Local surface shear stress
τ_S'	Spatial average surface shear stress on area S'
τ_S''	Spatial peak surface shear stress

1 Introduction

Desertification driven by wind erosion, reduced accumulation of snow in arid regions or the development of dust storms entering areas with a high population density are all examples of the influences of aeolian processes on our steadily changing environment. During the last decade, numerical modelling of such aeolian processes to predict, for example, local water

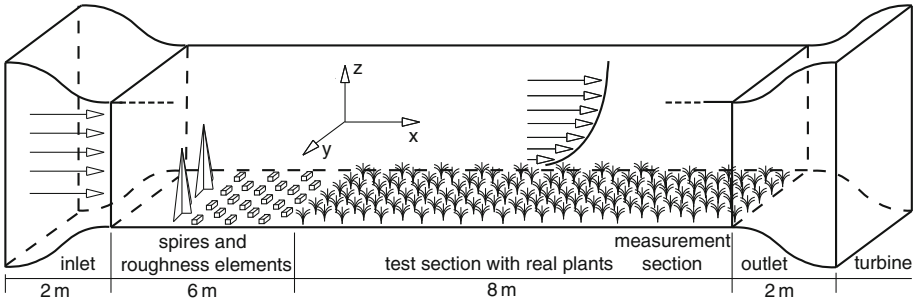

Fig. 1 Sketch of the SLF boundary-layer wind tunnel

storage as snow in arid regions, or the aggravation of desertification, has become significant in the environmental sciences. Model validation by means of experiments is essential to verify the accuracy of predictions. Often, experiments are also necessary to determine model parameters.

The local surface shear stress $\tau_S\,(x,\,y)$, acting on the ground beneath plant canopies, is the key parameter when identifying the shelter capability of vegetation against particle erosion and when modelling aeolian processes. Here, x is the streamwise and y the transverse direction of the flow (Fig. 1). The spatial peak surface shear stress τ_S'' defines the onset of erosion whereas most sediment transport models use the average friction velocity $u_* = (\tau/\rho)^{1/2}$ on a surface to determine the magnitude of the particle mass fluxes (e.g., Bagnold 1941). Raupach (1992) and Raupach et al. (1993) developed a model that allows for the prediction of the total stress τ as well as the peak $\left(\tau_S''/\tau\right)^{1/2}$ and the spatial average $\left(\tau_S'/\tau\right)^{1/2}$ shear-stress ratio as a function of a set of parameters that describe the geometric and the aerodynamic roughness of the surface. This model has been repeatedly tested by means of several wind-tunnel and field studies (Marshall 1971; Musick et al. 1996; Wolfe and Nickling 1996; Wyatt and Nickling 1997; Crawley and Nickling 2003; King et al. 2006; Gillies et al. 2007; Brown et al. 2008). However, all these studies are either from the field mainly using live plants with the limitation that flow conditions could not be controlled, or from wind tunnels using rigid and non-porous plant imitations, which often (but not always, as will be shown in this study) poorly reflect the aerodynamic behaviour of live vegetation. Such plant imitations often result in strong differences in the surface shear-stress distributions $\tau_S\,(x,\,y)$ and in the peak surface shear stress τ_S'' on the ground compared to live plants (Walter et al. 2012b). The highly irregular structures of live plants can be extremely flexible and porous allowing them to streamline with the flow. Hence, live plants cause considerable differences in the drag and flow regimes (e.g., Gromke and Ruck 2008) as well as in the size of the shed eddies compared to rigid and non-porous imitations.

The model of Raupach (1992) and Raupach et al. (1993) incorporates up to four parameters and fits any of the data of the different experiments from the literature reasonably well. Unfortunately, as a result, the range of possible values for the parameters obtained from the studies cited above is relatively large because of different experimental set-ups and roughness elements used. This makes it difficult for modellers to identify appropriate values for a specific vegetation canopy or surface with non-erodible roughness elements. Furthermore, no study systematically investigated how well the model predicts the differences in the shear-stress ratios for different kinds of roughness element such as cubes, cylinders, hemispheres or live plants. Most studies used solely one kind of roughness element, sometimes of different

size, to obtain variations in the roughness density λ, here defined as the roughness element frontal area A_f divided by the ground area S per roughness element. An intercomparison between the studies is often restricted by the varying experimental designs and measurement techniques deployed, resulting in disparate measurement accuracies. Some studies used Irwin sensors (Irwin 1981) or drag plates to measure the surface shear stress (e.g., Crawley and Nickling 2003; Brown et al. 2008) whereas other studies determined the friction velocity at the onset of particle entrainment from observed wind profiles (e.g., Marshall 1971; Musick et al. 1996).

This study presents an application and extension of Raupach's model to surface shear-stress measurements in live plant canopies of a single species (*Lolium perenne*) of varying roughness density and arrays of rectangular blocks to investigate and discuss the research gaps identified above. Model parameters a priori determined according to their definition are compared to their corresponding values obtained from least-square fits to the stress-ratio data as well as to literature values. The ability of the model to predict the total stress τ, the peak $\left(\tau_S''/\tau\right)^{1/2}$ and the average $\left(\tau_S'/\tau\right)^{1/2}$ shear-stress ratios for the plant canopies and the block arrays is tested. Finally, a model modification is presented that improves and facilitates its applicability in predicting peak stress ratios $\left(\tau_S''/\tau\right)^{1/2}$ and suggests replacing the problematic m parameter with a more universal parameter.

2 Background and Theory

Schlichting (1936) first defined the shear-stress ratio for a rough surface as $\tau = \tau_S + \tau_R$ where τ is the total stress on the entire canopy, τ_S is the average surface shear stress on the ground beneath the roughness elements and τ_R is the stress on the roughness elements. A model that predicts the stress ratio $(\tau_R/\tau)^{1/2} = a_1 \ln(1/\lambda) + a_2$ as a function of the roughness density λ and two fit parameters a_i was presented by Wooding et al. (1973), but fails for $\lambda > 0.05$ (Raupach 1992). Arya (1975) presented a model for two-dimensional roughness elements transverse to the mean wind that states $(\tau_R/\tau)^{1/2} = [1 + (1 - a_3\lambda)/(\lambda C_R/C_S)]^{-1}$ and Raupach (1992) presented an analytical treatment for predicting the total stress τ and the shear-stress ratio $(\tau_R/\tau)^{1/2} = (\beta\lambda/(1+\beta\lambda))^{1/2}$ and thus $(\tau_S/\tau)^{1/2} = (1/(1+\beta\lambda))^{1/2}$ for three-dimensional roughness elements. Here, $\beta = C_R/C_S$ is the ratio of the roughness element and the surface drag coefficient. The model of Arya (1975) predicts the stress ratio as well as the model of Raupach (1992) except at $\lambda > 0.1$ where Arya's model predicts $\tau_R/\tau > 1$, which is physically implausible. The widely accepted model of Raupach (1992) and Raupach et al. (1993) is entirely based on physically defined parameters and allows the prediction of the stress ratios τ_R/τ and τ_S/τ for different rough surfaces by determining solely β and λ. It must be noted that the roughness density λ is a geometric value that can easily be determined whereas the drag coefficients C_R and C_S, which define β, are flow dependent properties of the surface and the roughness elements. The drag force on an isolated roughness element can be written as

$$\Phi = \rho C_R b h U_h^2 \tag{1}$$

and defines C_R (Raupach 1992). Here, ρ is the air density, U_h is the mean wind velocity at the roughness element height h and b is the roughness element width. Raupach (1992) further defined an unobstructed drag coefficient C_S for the substrate surface such that:

$$\tau_S(\lambda = 0) = \rho C_S U_h^2. \tag{2}$$

The model of Raupach is further based on the definition of an effective shelter area A and shelter volume V as well as on two hypotheses. The effective shelter area A is defined as "the area in the wake of the roughness element in which the stress on the ground τ_S must be set to zero, to produce the same integrated stress deficit as that induced by the sheltering element" (Raupach 1992). "The effective shelter volume V describes the effect of a given roughness element upon the drag forces on other elements in its vicinity. It is the volume within which the drag force on the array of test obstacles must be set to zero, to produce the same integrated force deficit as induced by the sheltering element" (Raupach 1992). Hypothesis I states that the assumed wedge-shaped shelter area A and shelter volume V scale according to:

$$A = c_1 b h U_h / u_*, \tag{3}$$

$$V = c_2 b h^2 U_h / u_*, \tag{4}$$

where u_* is the friction velocity and c_1 and c_2 are constants of proportionality of $O(1)$. Hypothesis II states that "when roughness elements are distributed uniformly or randomly across a surface, the combined effective shelter area or volume can be calculated by randomly superimposing individual shelter areas or volumes" (Raupach 1992). The above definitions and hypotheses are then used to determine the surface shear stress τ_S and the stress on the roughness elements τ_R according to:

$$\tau_S = \rho C_S U_h^2 \exp\left[-c_1 \left(\frac{U_h}{u_*}\right) \lambda\right], \tag{5}$$

$$\tau_R = \lambda \rho C_R U_h^2 \exp\left[-c_2 \left(\frac{U_h}{u_*}\right) \lambda\right]. \tag{6}$$

The model thus allows for the prediction of the total stress $\tau = \tau_S + \tau_R$ on the entire surface using Eqs. 5 and 6, which results in an implicit equation for u_*. To solve this equation the assumption $c_1 = c_2 = c$ is made, which can be interpreted as "the elements shelter the ground and each other with the same efficiency" (Raupach 1992). This finally results in the implicit equation for U_h/u_*:

$$\frac{U_h}{u_*} = (C_S + \lambda C_R)^{-1/2} \exp\left[\frac{c\lambda}{2} \left(\frac{U_h}{u_*}\right)\right]. \tag{7}$$

The stress-ratio prediction of Raupach can then be obtained by using Eqs. 5 and 6 and assuming again $c_1 = c_2 = c$:

$$\frac{\tau_S}{\tau} = \frac{1}{1 + \beta\lambda}, \tag{8a}$$

$$\frac{\tau_R}{\tau} = \frac{\beta\lambda}{1 + \beta\lambda}. \tag{8b}$$

In Eq. 8a, τ_S is the average surface shear stress on the total surface area S rather than on the exposed surface area S'. Raupach et al. (1993) suggested the average surface shear stress on the exposed surface area S' to be $\tau'_S = \tau_S / (1 - \sigma\lambda)$ where σ is the ratio of the roughness element basal area to frontal area and $\sigma\lambda = 1 - S'/S$ is the basal area index (the basal area per unit ground area). This results in:

$$\left(\frac{\tau'_S}{\tau}\right)^{1/2} = \left(\frac{1}{(1 - \sigma\lambda)(1 + \beta\lambda)}\right)^{1/2}. \tag{9}$$

Equation 9 was validated by various measurements and investigations (e.g., Marshall 1971; Crawley and Nickling 2003). Raupach et al. (1993) further argued that not the

spatially-averaged τ_S' but rather the spatial peak surface shear stress τ_S'' at any location on the surface is responsible for the initiation of particle erosion. According to this, a rather empirical assumption on the relation between τ_S'' and τ_S' was made due to the limited surface shear-stress data available at that time. Raupach et al. (1993) defined that τ_S'' for a surface with roughness density λ is equal to τ_S' for a less dense (lower λ) rough surface composed of the same roughness elements:

$$\tau_S''(\lambda) = \tau_S'(m\lambda), \tag{10}$$

where, m is supposed to be a constant ≤ 1, which accounts for the difference between τ_S'' and τ_S'. This finally results in an equation for the peak surface shear-stress ratio:

$$\left(\frac{\tau_S''}{\tau}\right)^{1/2} = \left(\frac{1}{(1 - m\sigma\lambda)\,(1 + m\beta\lambda)}\right)^{1/2}. \tag{11}$$

Equation 11 has been validated by several wind-tunnel and field experiments (e.g., Musick and Gillette 1990; Musick et al. 1996; Wolfe and Nickling 1996; Wyatt and Nickling 1997; Crawley and Nickling 2003). However, most studies used estimated values of C_R and C_S to determine the parameter β and applied best fit methods to obtain m. Wyatt and Nickling (1997) found $m = 0.16$ for sparse desert creosote communities whereas Crawley and Nickling (2003) found $m = 0.5{-}0.6$ for solid cylindrical roughness elements with a slight dependency of m on wind speed. They further found a strong overestimation of the stress-ratio prediction (Eq. 11) when using m values obtained from the independent parameter definition (Eq. 10). Brown et al. (2008) found that the prediction (Eq. 11) works equally well for both staggered roughness element arrangements and for more randomly arranged surface features. However, all these studies show that the m parameter is not universal. Furthermore, the model of Raupach is based on a scaling argument (Eqs. 3 and 4) and ceases to behave sensibly for U_h/u_* (Eqs. 3 and 4) at roughness densities larger than about $\lambda \approx 0.1 - 0.3$ (Raupach 1992). Shao and Yang (2005, 2008) presented extensions of the model for high roughness densities $\lambda > 0.1$ with the argument that it is not clear how the effective shelter areas and volumes superimpose at higher roughness densities.

3 Methodology

Measurements of surface shear-stress distributions $\tau_S\,(x, y)$ on the ground beneath live plant canopies and rigid block arrays of different roughness densities λ were performed in the SLF atmospheric boundary-layer wind tunnel (Walter et al. 2009, 2012a,b). The wind tunnel (Fig. 1) is 14 m long, has a cross-section of 1 m × 1 m and has been used mainly in winter for investigating saltation, ventilation and the aerodynamic roughness length of naturally fallen snow (Clifton et al. 2006, 2008; Clifton and Lehning 2008; Guala et al. 2008; Gromke et al. 2011) and in summer to investigate the sheltering effect of live plants against soil erosion (Burri et al. 2011a,b).

The 8-m long test section covered with live plants allows for the generation of a natural boundary-layer flow (Walter et al. 2009). The wooden blocks (rectangular blocks with square basal cross-section of 40 mm × 40 mm and height of 80 mm) and the live plants (species: *Lolium perenne*, height: 100 mm) were arranged in staggered rows on the wind-tunnel floor (Fig. 2a, b). Four different roughness densities were investigated: 0, 5.25, 24.5, 55 plants or blocks m^{-2}, hereafter referred to as smooth-floor, the low-, medium- and high-density cases, respectively, with $\lambda = 0.017$, 0.087 and 0.200 for the plants (still air) and $\lambda = 0.017$, 0.078

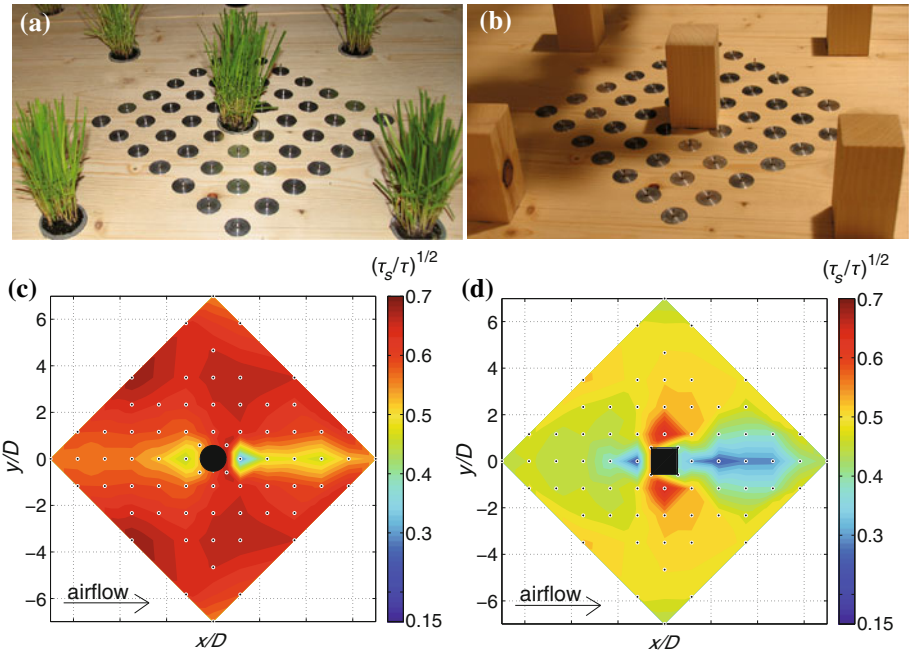

Fig. 2 Irwin sensors flush mounted with the wooden wind-tunnel floor for the medium density **a** live plant canopy (still air $\lambda = 0.087$) and **b** wooden block array ($\lambda = 0.078$). **c**, **d** The surface shear-stress distribution $(\tau_S/\tau)^{1/2}$ for the low density plant canopy ($\lambda = 0.017$) and wooden block array ($\lambda = 0.017$) at $U_\delta = 12\,\mathrm{m\,s^{-1}}$ [$D = 40\,\mathrm{mm}$; taken from Walter et al. (2012b)]

and 0.176 for the blocks. These configurations were investigated at three different freestream velocities $U_\delta = 8$, 12 and $16\,\mathrm{m\,s^{-1}}$ to systematically determine the differences in the shear-stress ratios when using live plants rather than rigid and non-porous plant imitations. All measurements were performed at the downwind end of the test section. A 6-m long fetch with spires and additional artificial roughness elements was used upwind of the test section for preconditioning the boundary-layer flow (Fig. 1). The boundary-layer thickness was about $\delta = 500\,\mathrm{mm}$ and it was shown that the inertial sublayer was sufficiently developed (Walter et al. 2009).

Irwin sensors (Irwin 1981) were mounted flush with the wind-tunnel floor in an array surrounding a roughness element to measure the surface shear-stress distribution $\tau_S\,(x, y)$ (Fig. 2a, b). The pressure differences at the sensors were measured using a custom made 32-channel pressure scanner (sampling rate: 200 Hz). Flow characteristics such as vertical profiles of the mean wind velocity u and the kinematic Reynolds stress $-\overline{u'w'}$ were measured using two-component hot-film anemometry (model: *Dantec Streamline*; sampling rate: 20 kHz) to determine the total stress $\tau = \rho u_*^2 = -\rho\overline{u'w'}$ in the constant stress layer above the canopy, and to ensure that a well-developed boundary layer was generated (Walter et al. 2012b). Two-component hot-film anemometers are known to underestimate the kinematic Reynolds stress $-\rho\overline{u'w'}$ in highly turbulent flows (Raupach et al. 1991). However, our kinematic Reynolds stress profiles (as presented in Walter et al. 2012b) suggest no measurement problems in the constant-stress layer above the plant canopies and block arrays where u_* was determined. All shear stress and velocity values are 30 s time averaged.

Figure 2c, d shows the surface shear-stress distribution $\tau_S\,(x, y)$ as a fraction of the total stress τ for the low-density plant and block case at a freestream velocity of $U_\delta = 12\,\mathrm{m\,s^{-1}}$ (taken from Walter et al. 2012b). The accuracy of the skin friction velocity $u_\tau = (\tau_S/\rho)^{1/2}$ measurements averages to about $\pm 5\,\%$ for $u_\tau > 0.13\,\mathrm{m\,s^{-1}}$ (Walter et al. 2012a). Additional details on the experimental set-up and the measurements can be found in Walter et al. (2009, 2012b). The accuracy of the Irwin sensor and the hot-film measurements are discussed in detail in Walter et al. (2012a).

4 Results and Discussion

4.1 Total Stress Prediction

To predict the total stress $\tau = \rho u_*^2$ on a canopy with non-erodible roughness elements using Eq. 7, the roughness element and the surface drag coefficients C_R and C_S, the roughness density λ, the mean velocity U_h at the top of the roughness elements and the constant of proportionality c need to be known.

Some studies (e.g., Brown et al. 2008) determined C_R and C_S by measuring the force on a single, wall-mounted roughness element and the surface using drag plates. However, in this study, the force Φ (Eq. 1) on a single roughness element was estimated using the difference between the total stress τ above and the surface shear stress τ_S' on the exposed surface area S' for the low-density case (5 roughness elements per m^2, $\lambda = 0.017$) with an isolated roughness flow regime to estimate C_R according to:

$$\Phi = \rho C_\mathrm{R} b h U_h^2 \approx \tau S - \tau_S' S'. \tag{12}$$

That an isolated roughness flow is obtained in the low roughness density case is substantiated by the fact that the shelter areas downwind of the roughness elements do not reach the next element (Fig. 2c, d; Walter et al. 2012b). The surface drag coefficient C_S was determined using Eq. 2 and the average surface shear stress τ_S measured with 32 Irwin sensors for the smooth-floor case. This method used to determine C_R and C_S, however, does not check the full momentum balance as investigated by Marshall (1971) but results in reasonable values for the drag coefficients as will be shown later.

Figure 3 shows the drag coefficients for the plant and the block cases. In the plant case, three different values for C_R and C_S were determined at the freestream velocities $U_\delta = 8$, 12 and $16\,\mathrm{m\,s^{-1}}$ showing the influence of the plants ability to streamline with the flow resulting in slightly smaller plant drag coefficients C_R at higher roughness element Reynolds numbers $Re_h = U_h h/\nu$; here, ν is the kinematic viscosity of air. This C_R (Re_h) dependency is similar to that of fountain grass as found by Gillies et al. (2002), although their drag coefficients are larger most likely because of more voluminous plants. The drag coefficient C_R in the block case is about 35 % greater than in the plant case, which can be explained by the rigid and non-porous shape of the block, and suggests a greater flow resistance for the blocks than for the plants. The surface drag coefficient C_S for the plants remains constant ($C_\mathrm{S} \approx 0.0018$) at higher wind velocities suggesting Reynolds number independency. Note the different scaling for C_R (left-side ordinate) and C_S (right-side ordinate) in Fig. 3. The surface drag coefficient $C_\mathrm{S} = 0.0019$ determined for the block case is slightly greater compared to the plant case because the height and thus the wind velocity U_h are slightly greater for the plant than for the block (Eq. 2). The roughness length of the wooden substrate surface is of the order of magnitude of $z_0 = 0.01$ mm and was determined by fitting the logarithmic law to the mean velocity profile $u(z)$ measured with the two component hot-film anemometer. Combining

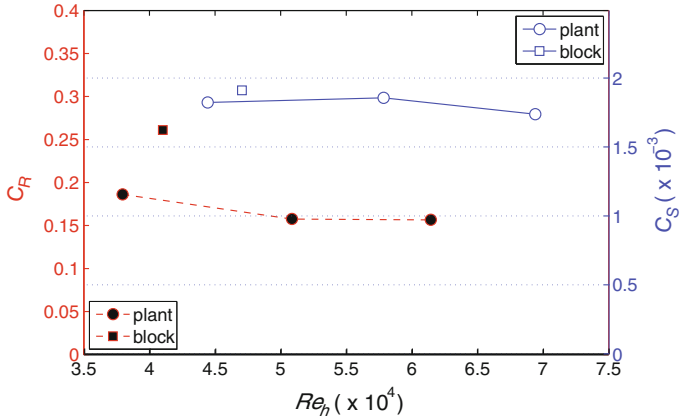

Fig. 3 Roughness element drag coefficient C_R and surface drag coefficient C_S for the plant cases (as a function of the Reynolds number Re_h) and the block case (at $U_\delta = 12\,\mathrm{m\,s^{-1}}$)

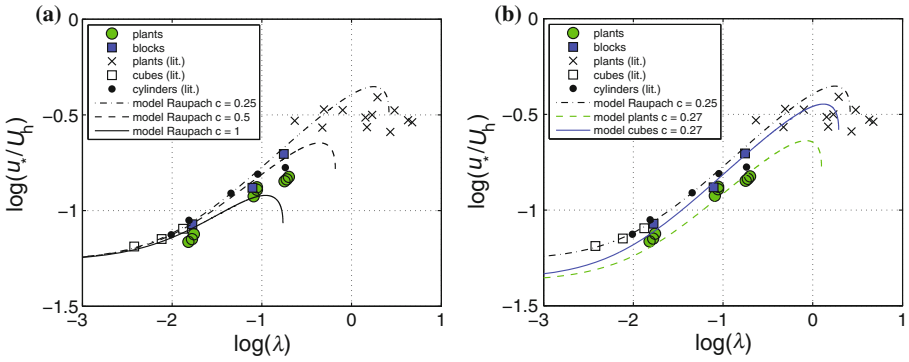

Fig. 4 Normalized friction velocity u_*/U_h as a function of the roughness density λ for the plant and block cases together with literature data and the model of Raupach (1992): **a** using the original model parameters $C_R = 0.3$, $C_S = 0.003$ and c from Raupach (1992), and **b** using individually determined drag coefficients: $C_R = 0.166$ and $C_S = 0.0018$ for the plants and $C_R = 0.261$ and $C_S = 0.0019$ for the blocks. $c = 0.27$ has been chosen for both the plant and the block cases for better comparison

Eq. 2 with the logarithmic law allows the determination of the surface drag coefficient C_S. The resulting drag coefficient is $C_S = 0.0017$ (with $z_0 = 0.01$ mm) for the plant case, which agrees very well with the drag coefficients from Fig. 3. To obtain the roughness density λ, the frontal area A_f of the plants was determined by digital image analysis of front view pictures of the plants at different wind velocities (Walter et al. 2012b). This analysis shows a decrease in A_f and thus in λ for higher wind velocities for each density case (see Appendix). For the remaining parameter c (Eq. 7), Raupach (1992) suggested a constant of proportionality of $O(1)$ and used $c = 0.25, 0.5$ and 1 for his plots to illustrate the influence of c on the total stress prediction.

Figure 4a shows the normalized friction velocity $u_*/U_h = \left(\tau/\rho U_h^2\right)^{1/2}$ for our plant and block canopies against the roughness density λ together with literature data taken from Raupach (1992) and Raupach's model (Eq. 7). The block data agree well with the literature data for cubes, cylinders and different vegetation canopies validating our measurements. It

needs to be mentioned that the data for the different roughness elements from the literature do not overlap at different λ ranges. This inhibits a clear identification of roughness element shape, porosity or flexibility effects on the total stress generation. Because of the limited data available, Raupach (1992) used generalized drag coefficients $C_R = 0.3$ and $C_S = 0.003$ for all three kinds of roughness elements to apply the model (Eq. 7). Although the model of Raupach fits the literature data and our block data satisfactorily well, the fact that our C_R values for the plants do not agree with the generalized value of $C_R = 0.30$ assumed by Raupach (1992) results in a poor agreement of the model with our plant data (Fig. 4a). Furthermore, the range of possible values for c defined in Raupach (1992) still remains relatively large, between $0.25 < c < 1$.

An improved agreement of the model with our plant and block data was found when using the individual drag coefficients C_R and C_S from Fig. 3 (Fig. 4b). A Re_h-averaged C_R value ($C_R = 0.166$) was used in the plant case to obtain a clearer picture. This is justified because the measurement inaccuracies in u_*/U_h and λ are larger than the changes of the model prediction when implementing a Reynolds-number dependent drag coefficient C_R (Re_h) for the plants (not shown here). The model is able to predict the difference in total stress generation between the two different kinds of roughness elements correctly. Here, the parameter c was used as an independent best-fit parameter where $c = 0.29 \pm 0.03$ was found for the plants and $c = 0.25 \pm 0.04$ for the blocks, and where all errors presented here are given as one standard deviation. This suggests that the constants of proportionality $c_1 = c_2 = c$ of Raupach's model, which connect the size of the effective shelter area and volume to the flow parameters U_h and u_* (Eqs. 3 and 4), can be given a value of about $c = 0.27$. This value of $c = 0.27$ was used for the model in Fig. 4b to achieve a better qualitative comparison.

4.2 Shear-Stress Partitioning

In this section, a straightforward application of Raupach's stress-ratio prediction model (Eqs. 9 and 11) to our plant and block measurements using model parameters a priori determined according to their definition is presented. Earlier studies (e.g., Marshall 1971; Brown et al. 2008) applied Raupach's model to solely one kind of roughness element. However, since the model contains up to four parameters, it can be tuned to fit any data well if one or more of those parameters are reasonably adjusted. The following analyses show that the model is capable of predicting the differences in stress ratio for different roughness elements correctly when using the independently determined model parameters.

4.2.1 Average Stress Ratio

The average shear stress τ'_S on the exposed surface area S' beneath a canopy is an important measure to estimate the overall sheltering capability of non-erodible roughness elements. Figure 5 shows the average stress ratio $\left(\tau'_S/\tau\right)^{1/2}$ for the plant and the block experiments as a function of the roughness density λ together with literature values from similar studies (Marshall 1971; Lyles and Allison 1975; Crawley and Nickling 2003). Despite a good overall agreement of our data with the literature values, significant differences were found between the stress ratios of the plants and the blocks at a constant roughness density λ. Furthermore, the blocks provide the lower stress ratio at low roughness densities relative to the plants. This changes for the high roughness density case where the plants provide the lower stress ratios relative to the blocks. The different freestream velocities $U_\delta = 8$, 12 and 16 m s^{-1} in the plant case result in three different data points for each canopy density in Fig. 5. Note that the slightly lower roughness densities λ at higher freestream velocities U_δ are a result of the

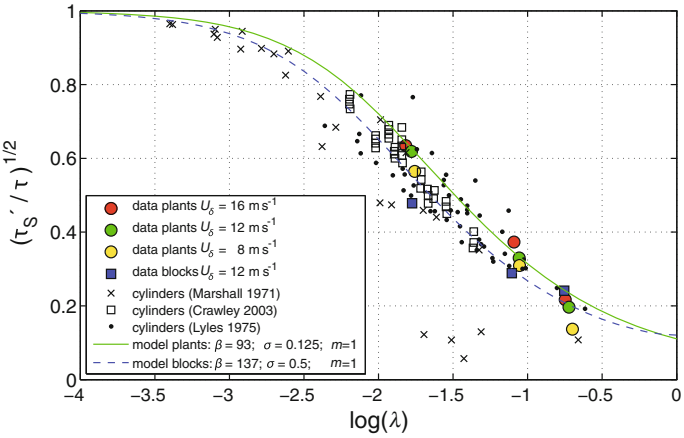

Fig. 5 Average surface shear-stress ratio $\left(\tau_S'/\tau\right)^{1/2}$ as a function of the roughness density λ. Measurement and literature data together with a straightforward application of Raupach's model using model parameters determined according to their definition

decreased frontal areas A_f of the plants (see Appendix). This results in higher flow velocities close to the ground and higher surface shear forces with slightly higher average stress ratios $\left(\tau_S'/\tau\right)^{1/2}$.

Parameters σ and β, determined a priori from their definition, were used to assess the performance of Raupach's model (Eq. 9) in predicting the stress ratio $\left(\tau_S'/\tau\right)^{1/2}$ (Fig. 5). The basal to frontal area index σ is $\sigma = 0.5$ in the case of the blocks and was estimated as $\sigma \approx 0.125$ in the case of the plants. Because the plants streamline with the flow, σ slightly increases by about 30 % for higher wind velocities. However, σ significantly affects the stress-partition prediction only at roughness densities higher than our high density case ($\lambda > 0.2$) (Raupach et al. 1993). The value of $\sigma = 0.125$ for the plants has thus been used for any calculation presented in this study. The parameter $\beta = C_\mathrm{R}/C_\mathrm{S}$ was calculated using the values from the previous section (Fig. 3) and is $\beta = 137$ for the blocks and $\beta = 93$ for the plants when using again a Re_h-averaged C_R value for the plants, for the same reasons as before. For comparison, the model has been applied with β as an independent least-square fit parameter where $\beta = 167 \pm 67$ was found for the blocks and $\beta = 107 \pm 10$ for the plants. These values are both about 15 % larger than the independently determined values from the previous section, which can be explained by the influence of the isolated roughness flow that seems to result in a slight underprediction of the β parameter. Please note that the correct determination of C_R strictly requires flow around a single surface-mounted roughness element.

Figure 5 shows that the model is able to predict the general difference between the two different roughness elements for low λ and supports the statement of Raupach (1992) that the shear-stress ratio is fully controlled by the β parameter. However, the model does not reflect the fact that the plants provide the lower stress ratio $\left(\tau_S'/\tau\right)^{1/2}$ for the high roughness density case ($\lambda \approx 0.18$) while for the low density case ($\lambda \approx 0.017$) the blocks provide the lower stress ratio. This reversal in the sheltering effect at high roughness densities is relatively small and thus needs to be interpreted with caution. However, it is an important finding and the reversal itself as well as the reasons why it is not captured by the Raupach model can be explained: first, the Raupach model is expected to become progressively worse for λ

larger than about 0.1–0.3 for theoretical reasons (Shao and Yang 2008). However, the model predictions generally agree with our data even for the high density case suggesting a limiting value for the model of $\lambda > 0.2$. Secondly, the model of Raupach does not account for the streamlining behaviour and the fluttering capability of the plants. The streamlining effect of the plants results in generally less flow resistance (which implies an effectively smaller u_*) compared to the blocks at the low and medium roughness densities (e.g., Walter et al. 2012b). For the high density case, the blocks result in a skimming flow regime with a reduced flow resistance (smaller u_*) compared to the medium density block case (Walter et al. 2012b). This supports the above assumption that our high density block case might fall within the range where Raupach's model starts to become invalid. This decrease in u_*, however, has not been found for the plants. The fluttering capability of the plants has the opposite effect of the streamlining behaviour in that it is able to enhance the flow resistance. This effect is strongest for the high density plant case, because of the large amount of plants, and explains the higher total stress production (larger u_*) relative to the high density block case (Walter et al. 2012b). Moreover, the streamlining effect of the plants results in a higher horizontal coverage of the surface compared to the blocks and is also strongest in the high density case. This is a specific effect resulting from our highly flexible plant species and may well be different for rigid shrubs. However, the horizontal coverage is the reason why a lower average surface shear stress τ_S' was found for the high density plant case compared to the block case (Walter et al. 2012b). The latter effect, together with the higher total stress τ generated by the plants compared to the blocks in the high density case, explains the reversal in the stress ratio $\left(\tau_S'/\tau\right)^{1/2}$.

One way to implement this reversal into Raupach's model would be to introduce additional parameters to account for the horizontal coverage and the fluttering capability of the plants. However, since the model already contains parameters that are still relatively unspecified and difficult to determine for various canopies, an inclusion of additional parameters was not considered. The above discussion points out that characteristics such as the porosity, the flexibility and the shape of the roughness elements can have complex influences on the stress partition and its dependency on λ. Accordingly, results based on measurements using rigid and non-porous plant imitations have to be considered cautiously when estimating the shelter capability of live plant canopies.

4.2.2 Peak Stress Ratio

Figure 6 shows the peak surface shear-stress ratio $\left(\tau_S''/\tau\right)^{1/2}$ as a function of λ for the plant and the block experiments together with literature data and the results from the Raupach model (Eq. 11) applied to our data. An overall agreement of our data with the relative widely spread ensemble of literature data is obtained. Interestingly, our plant and block peak stress ratios $\left(\tau_S''/\tau\right)^{1/2}$ are similar for the different roughness densities, at least for the low and the medium density cases, and can be explained as follows. The rigid and non-porous blocks result in a stronger flow deflection around their body compared to the flexible and porous plants. Hence, the higher wind velocities in the speed-up zones at both sides of the blocks result in higher peak surface shear-stress values τ_S'' relative to the plants. However, the stronger flow deflection in the block case also causes a higher flow resistance and thus a higher total stress τ on the entire block array compared to the plant canopy. This suggests that peak surface shear-stress ratios $\left(\tau_S''/\tau\right)^{1/2}$ obtained by measurements using rigid and non-porous plant imitations can be quite similar to those for real vegetation canopies. Thus, artificial plant imitations might satisfactorily represent real canopies considering investigations of the

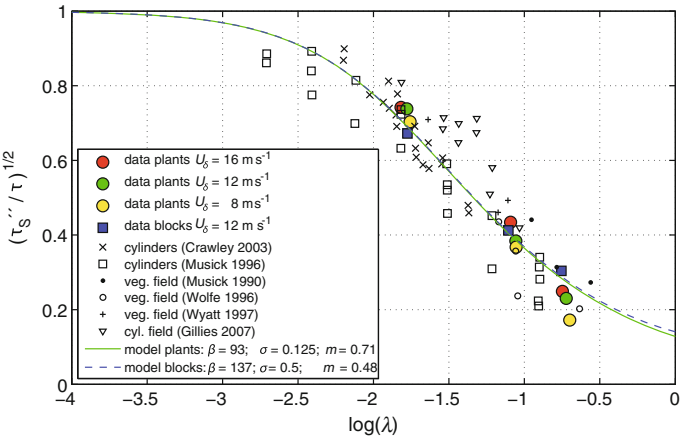

Fig. 6 Peak surface shear-stress ratio $\left(\tau_S''/\tau\right)^{1/2}$ as a function of the roughness density λ. Measurement and literature data together with a best fit application of Raupach's model with m as the independent fit parameter

peak stress ratio $\left(\tau_S''/\tau\right)^{1/2}$. Nevertheless, the spatial distributions and the absolute values of $\tau_S(x, y)$ can be very different for canopies with plant imitations such as rigid and non-porous obstacles compared to live plant canopies (Walter et al. 2012b). The same reversal in the sheltering effect from low to high roughness densities as found for the average stress ratio was found for the peak stress ratio and can be made plausible with similar arguments as discussed in the previous section.

The application of the Raupach model (Eq. 11) with m as an independent least-square fit parameter results in $m = 0.48 \pm 0.07$ ($R^2 = 0.991$) for the blocks and $m = 0.71 \pm 0.08$ ($R^2 = 0.957$) for the plants. Wyatt and Nickling (1997) found $m = 0.16$ for sparse desert creosote communities in field experiments, which is a relatively small value compared to the findings of other studies where $0.4 < m < 0.6$ was found for cylinders or blocks (e.g., Crawley and Nickling 2003; Brown et al. 2008). Crawley and Nickling (2003) explained this difference as an effect of flow dynamics influenced by porous roughness elements. However, our data suggest that the blocks produce higher peak and lower average surface shear stresses than the plants due to the stronger flow deflection around the blocks for the low and the medium density cases. This in turn implies that the m value, according to its definition $\tau_S''(\lambda) = \tau_S'(m\lambda)$, has to be smaller for blocks than for plants as observed in our study. However, a direct comparison is difficult since Wyatt and Nickling (1997) used fairly different plants (*creosote bushes*) with a high porosity and low flexibility whereas the plants used in this study (*rye grass*) have high flexibility and a relatively low porosity.

4.3 The m Parameter

A similar approach as presented by Crawley and Nickling (2003) has been used to determine the m parameter according to its definition (Eq. 10). Therefore, in a first step, the peak τ_S'' and the average τ_S' surface shear stresses were plotted against the roughness density λ for a freestream velocity $U_\delta = 16\text{m s}^{-1}$ and logarithmic regression relations were applied (Fig. 7):

$$\tau_S' = a_1 \ln(\lambda) + b_1, \tag{13a}$$

$$\tau_S'' = a_2 \ln(\lambda) + b_2. \tag{13b}$$

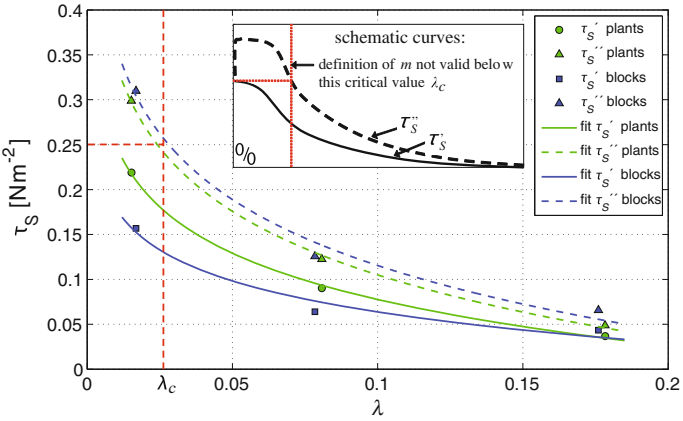

Fig. 7 Peak τ_S'' and average τ_S' surface shear-stress data as a function of the roughness density λ for the plant and the block experiments at $U_\delta = 16\,\mathrm{m\,s^{-1}}$. Logarithmic regression relations (Eq. 13) were applied to the data. Schematic curves are shown in the upper box to visualize the assumed behaviour of τ_S'' and τ_S' outside the measurement range

The independent least-square fit parameters are $a_1 = -0.074\,\mathrm{N\,m^{-2}}$ and $b_1 = -0.094\,\mathrm{N\,m^{-2}}$ $\left(R^2 = 0.999\right)$ and $a_2 = -0.102\,\mathrm{N\,m^{-2}}$ and $b_2 = -0.130\,\mathrm{N\,m^{-2}}(R^2 = 0.999)$ for the plant case. Identical analyses were made for $U_\delta = 8$ and $12\,\mathrm{m\,s^{-1}}$ (not shown here) to identify the dependency of the m parameter on the wind velocity or the Reynolds number Re_h, respectively. Logarithmic regression relations (Eq. 13) were used by Crawley and Nickling (2003) because of both a good fit and the convergence of τ_S'' and τ_S' for small ($\lambda \to 0$) and large ($\lambda \to 1$) roughness densities. These relations satisfactorily represent the dependency of τ_S'' and τ_S' on λ within the measurement range $0.015 < \lambda < 0.18$ (Fig. 7).

Schematic curves are shown in the upper box in Fig. 7 to visualize the expected dependency of τ_S'' and τ_S' on λ outside the measurement range for our kind of roughness elements. For both the plant and the block experiments, τ_S' converges against a constant value of $\tau_S' = 0.25\,\mathrm{N\,m^{-2}}$ for $\lambda \to 0$, which was measured for the smooth-floor case at a freestream velocity of $U_\delta = 16\,\mathrm{m\,s^{-1}}$. Below a critical roughness density λ_c, τ_S'' is expected to be larger than any τ_S' at $\lambda < \lambda_c$, so the parameter definition for m (Eq. 11) is not valid below λ_c (schematic curves in Fig. 7). Just as the last roughness element on a large unit ground area S is removed to achieve a roughness density $\lambda = 0$, a point of discontinuity occurs and $\tau_S'' = \tau_S'$. When decreasing the roughness element size to achieve lower roughness densities λ, the point of discontinuity vanishes and τ_S'' decreases steadily until it reaches τ_S' for $\lambda = 0$.

The peak surface shear stress τ_S'' can be even larger than the total stress τ at very low λ considering widely spaced roughness elements on a surface, with a strong deflection of the airflow resulting in locally very high wind velocities close to the ground in the speed-up zones. This is in conflict with the order suggested by Raupach et al. (1993), viz that $\tau_S < \tau_S' < \tau_S'' < \tau$; however, he already mentioned that assuming $\tau_S'' < \tau$ is a rather speculative assumption due to the lack of available data. That τ_S'' can be larger than τ results in enhanced erosion by the roughness elements at low canopy densities, as validated e.g. by Burri et al. (2011b).

For high roughness densities λ, both τ_S'' and τ_S' converge to zero (schematic curves in Fig. 7). This is obtained by the fact that $\ln(\lambda \to 1) = 0$ in Eq. 13 although the parameter b_i is needed to obtain reasonable fits. However, the values for a_i and b_i from the fits are all

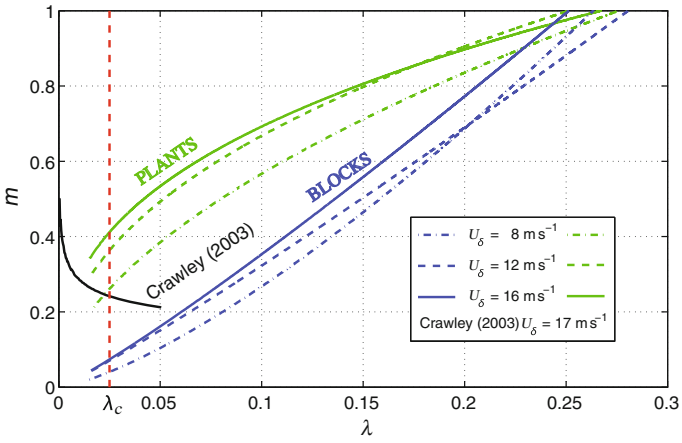

Fig. 8 Parameter m as a function of the roughness density λ and U_δ for the plant and the block cases. The curve from Crawley and Nickling (2003) for wooden cylinders is included as well. Our data are incorrect below $\lambda_c \approx 0.025$ (*dotted line*) because the definition for m is not valid below (see also Fig. 7)

slightly smaller than zero permitting τ_S' and τ_S'' to become zero for $\lambda < 1$. This is in agreement with literature results that suggest completely sheltered surfaces already for $\lambda > 0.3$ (e.g., Raupach 1992).

In a second step, an iterative comparison of τ_S'' with τ_S' from Fig. 7 over the entire λ range was carried out to evaluate Eq. 10 and to obtain the dependency of the m parameter on the roughness density λ (Fig. 8). This was done for the freestream velocities $U_\delta = 8$, 12 and 16 m s^{-1} and for both the plant and the block experiments. The $m(\lambda)$ curve determined by Crawley and Nickling (2003) for solid cylinders at a freestream velocity of $U_\delta = 17.07$ m s^{-1} is included as well for $\lambda < 0.0434$, which was the upper limit of their measurement range. Crawley and Nickling (2003) used different sizes of solid cylinders to obtain different roughness densities λ. As indicated in Fig. 8, Crawley's logarithmic regression relations result in $m(\lambda)$ converging against 1 for $\lambda \to 0$ as should be the case when reducing the roughness density λ by decreasing not just the number of roughness elements per unit area but also the roughness element size. In contrast, in our case and as mentioned before, τ_S' converges against our constant "smooth-floor" limit value of $\tau_S' = 0.25$ N m^{-2} for small roughness densities, while τ_S'' values significantly larger than τ_S' occur. This implies that below the critical value λ_c there is no corresponding $\tau_S'(m\lambda)$ to determine $\tau_S''(\lambda)$ according to Eq. 10 (schematic curves in Fig. 7). As a result, our $m(\lambda)$ curves are incorrect below $\lambda_c \approx 0.025$ (red dotted line in Fig. 8), which is larger than the lower limit of our measurement range ($\lambda = 0.017$). However, for the sake of completeness, the m values have been plotted down to $\lambda = 0.017$.

When predicting $m(\lambda)$ for larger roughness densities outside the measurement range ($\lambda > 0.18$), the fact that τ_S'' and τ_S' converge against zero and both become zero for a completely sheltered surface means that m has to converge against one. Our $m(\lambda)$ curves in Fig. 8 suggest that, in both the plant and the block cases and for all free-stream velocities U_δ, the surface becomes completely sheltered at a roughness density of $\lambda \approx 0.25$, i.e. when $m = 1$. This agrees with results presented by Raupach (1992) who found completely sheltered surfaces for $\lambda > 0.3$. Strictly, the $m(\lambda)$ curves should asymptotically converge against $m = 1$ and not cross it as in our case. However, this can be explained by the limited measurement accuracy as well as the limitations of the logarithmic regression relations from Eq. 13.

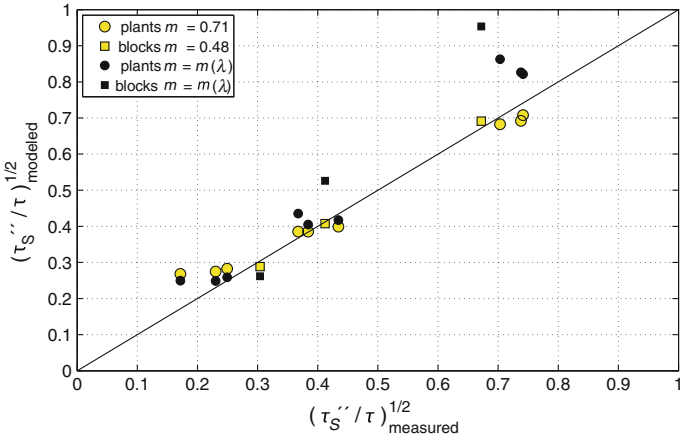

Fig. 9 Modelled against measured peak surface shear-stress ratios $\left(\tau_S''/\tau\right)^{1/2}$ when using a constant m parameter and when using $m = m\,(Re_h, \lambda,$ shape) from Fig. 8

When averaging the m values from Fig. 8 over the measured λ range, the average values for the plants are $m = 0.63, 0.69, 0.70$ and for the blocks $m = 0.37, 0.40, 0.44$ for the free-stream velocities $U_\delta = 8$, 12 and 16 m s^{-1}. These values agree quite well with the m values obtained by the least-square fit method given in Fig. 6 where $m = 0.71$ was found for the plants and $m = 0.48$ for the blocks. When using the least-square fit β values ($\beta = 107$ and 167 for the plants and the blocks as presented in Sect. 4.2.1) to obtain least-square fit m values, the values are $m = 0.61$ for the plants and $m = 0.39$ for the blocks.

Figure 8 shows that m is a function of U_δ or the Reynolds number Re_h, the roughness density λ and the roughness element shape (see also Crawley and Nickling 2003; Brown et al. 2008). Crawley and Nickling (2003) found that the model strongly overestimates the shear stress-ratio $\left(\tau_S''/\tau\right)^{1/2}$ when using their λ-dependent m parameter. Figure 9 shows the modelled versus the measured stress ratios: first when using the constant least-square fit m parameters from Fig. 6 ($m = 0.71$ and $m = 0.48$), and second when using $m = m(Re_h, \lambda,$ shape) from Fig. 8 for the model. An overall better agreement is found for the constant m parameter whereas the modelled data points in the high density plant case, i.e. for the lowest stress ratios, slightly improve when using $m = m(Re_h, \lambda,$ shape). For the medium roughness density, only the block data point deteriorates and in the low density case, i.e. for the highest shear-stress ratios, all modelled values deteriorate when using $m = m(Re_h, \lambda,$ shape). The latter can be explained by the fact that the $m(Re_h, \lambda,$ shape) values become physically not meaningful below $\lambda < \lambda_c$ because of the limitations of Eq. 10 at low roughness densities, as discussed earlier in this section (Figs. 7, 8). This suggests that an improvement of the predictability of Raupach's model can be accomplished when using $m(Re_h, \lambda,$ shape), at least for medium and high density canopies. However, determining $m(Re_h, \lambda,$ shape) using Eq. 10 is very difficult, time consuming and laborious suggesting that using a constant m parameter is more practicable.

For rigid cylinders, $m = 0.4{-}0.5$ has been found by earlier studies (e.g., Brown et al. 2008), which agrees very well with our rigid block values for m. For live plants, a large variation of possible m values ranging from $m = 0.16$ (Wyatt and Nickling 1997) to $m = 0.71$ (this study) has been found. The variation of the m parameter strongly affects the applicability of the model since it is difficult to choose an appropriate m value for a canopy of interest. To

determine the m parameter for a specific type of roughness elements, a very time consuming series of measurements at different roughness densities is required to obtain the constant m or the non-constant $m(Re_h, \lambda, \text{shape})$ parameter.

4.4 The Peak Mean Stress Ratio a

The model of Raupach becomes a useful tool if one can independently and easily determine the parameters σ, λ, β, and m to calculate the stress ratio for a certain canopy. The geometric parameters describing the roughness of the canopy, the frontal to basal area index σ and the roughness density λ are relatively easy to determine. Literature values for $\beta = C_R/C_S$ are available for different kinds of roughness elements (e.g., Gillies et al. 2002). Additionally, β can be determined by measuring the force Φ on a single wall-mounted roughness element using a force gauge to determine C_R (Eq. 1) and by measuring τ_S in the absence of any roughness elements using an Irwin sensor or other techniques (e.g., hot-film anemometry) to determine C_S (Eq. 2).

In the previous section it was shown that a large range of m has been reported ($m = 0.16{-}0.71$) and that it is cumbersome to determine m from fits of shear-stress ratio data (e.g., Fig. 6) or directly using the independent parameter definition (Eq. 10). It was shown that the non-constant $m(Re_h, \lambda, \text{shape})$ parameter is even more difficult to determine (Figs. 7, 8) and only improves the peak stress-ratio prediction when determined with high accuracy (Fig. 9). Furthermore, an extensive experimental set-up and high accuracy measurements of the surface shear-stress distribution are required to determine m adequately. These facts suggest that the m parameter according to its definition from Eq. 10 is rather impracticable and that there is a demand for a new, physically more solid, definition to describe the relation between the peak shear stress τ_S'' and the surface average shear stress τ_S'.

We suggest the definition of a new parameter a that linearly relates the peak shear stress τ_S'' to the surface average shear stress τ_S' instead of using the definition $\tau_S''(\lambda) = \tau_S'(m\lambda)$ (Eq. 10):

$$\tau_S'' = a\tau_S'. \tag{14}$$

This parameter is hereafter termed the peak mean stress ratio a. Crawley and Nickling (2003) presented a linear relationship between τ_S'' and τ_S' independent of λ and U_δ, while King et al. (2006) found a linear relation between $\left(\tau_S''/\tau\right)^{1/2}$ and $\left(\tau_S'/\tau\right)^{1/2}$, which means in fact the same as Eq. 14.

Figure 10 shows τ_S'' as a function of τ_S' for both the plant and the block experiments and for all measured roughness densities λ. For all cases, this relationship is independent of U_δ and strongly linear with $R^2 > 0.99$ on average. The strong linear dependency can be made physically plausible when considering the airflow close to the ground in between the roughness elements. First, it is assumed that the spatio-temporally averaged wind velocity inside the canopy $\langle U_i \rangle$ is driven by the airflow above and is linearly related to the freestream velocity U_δ. Second, we assume that there are no large changes in the spatial surface shear-stress distribution $\tau_S(x, y)$ when increasing U_δ, i.e. that the location of τ_S'' and the dimensions of the shelter area remain unaltered. These assumptions hold for a Reynolds-number independent flow. Since the friction velocity u_* is proportional to U_δ (neglecting the effects of thermal stratification), and hence the total stress τ is proportional to the square of the freestream velocity $\left(\tau \sim U_\delta^2\right)$, it can be assumed that the local surface shear stress $\tau_S(x, y)$ scales with $\langle U_i \rangle^2$ and thus with U_δ^2. Therefore, the peak and the average surface shear stress τ_S'' and τ_S' are assumed to be proportional to the square of the freestream velocity according to:

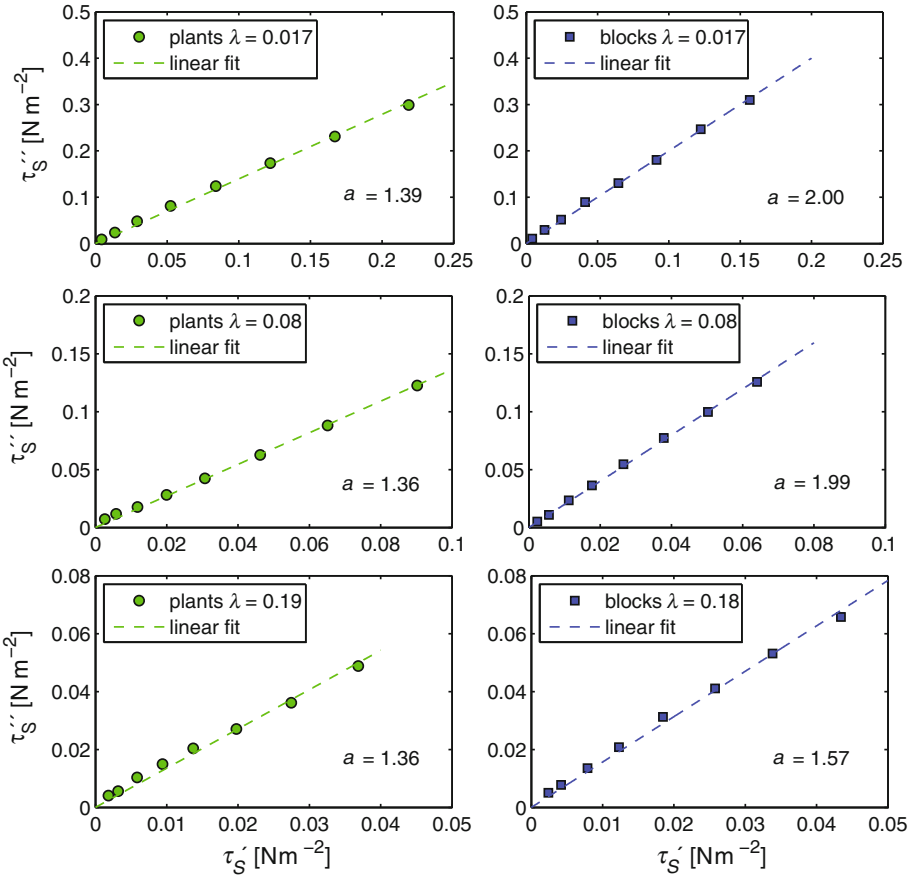

Fig. 10 Peak surface shear stress τ_S'' as a function of the average surface shear stress τ_S' for the plant and the block experiments and for different roughness densities λ. The eight data points in each plot correspond to free-stream velocities $U_\delta = 2{-}16\,\mathrm{m\,s^{-1}}$

$$\tau_S' = c' U_\delta^2, \tag{15a}$$

$$\tau_S'' = c'' U_\delta^2, \tag{15b}$$

where c' and c'' are constants of proportionality. This finally results in $\tau_S''/\tau_S' = c''/c' = a =$ constant as defined in Eq. 14 and substantiated by Fig. 10.

Further, the peak mean stress ratio a remains approximately constant for different roughness densities with $a = 1.39 \pm 0.02$, 1.36 ± 0.02 and 1.36 ± 0.04 for the low, the medium and the high density plant cases. For the blocks, a is constant for the low and the medium density cases with $a = 2.00 \pm 0.02$ and 1.99 ± 0.02 and decreases for the high density case to $a = 1.57 \pm 0.03$. This suggests that for sparse canopies (e.g. our low and medium density cases) with isolated roughness and wake interference flows (Walter et al. 2012b), the strength of the deflection of the airflow around the roughness elements and the sizes of the resulting eddies shed by the obstacles are independent of the inter-roughness element spacing and thus λ. The medium density cases are examples of wake interference flow because the sheltered areas reach the next roughness element downstream while a significant fraction of the surface

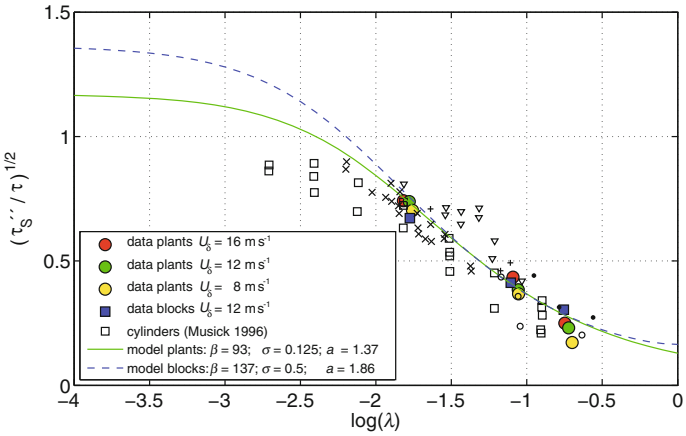

Fig. 11 Peak surface shear-stress ratio $\left(\tau_S''/\tau\right)^{1/2}$ as a function of the roughness density λ (same data as in Fig. 6). Measurement and literature data together with the modified model of Raupach from Eq. 16, which includes the new parameter a with values determined using its definition from Eq. 14

remains unsheltered (Walter et al. 2012b). The lower value of $a = 1.57$ found for the high density block case suggests that this is no longer true for high roughness densities with a skimming flow regime. This can be explained by the smaller eddies that are shed due to the influence of the neighbouring obstacles, which limit the space in between the roughness elements. That this is not the case for the high density plant case and a is still the same as for the low and the medium density case is attributed to the fact that the eddies shed by grass swards of the plants in our case are relatively small compared to the inter-roughness element spacing even for the high density case. This hypothesis is supported by Walter et al. (2012b), who found that no large horseshoe vortices develop in the plant case. To summarize, the data suggest that for live vegetation canopies the peak-mean stress ratio a (Eq. 14) is independent of λ and U_δ or Re_h respectively, and that a only depends on the roughness element shape itself: $a = a(\text{shape})$. This is a big advantage compared to the m parameter, which depends on λ, Re_h and the shape as shown in Sect. 4.3. Consequently, a is easier to determine for different vegetation species then m. That a is independent of Re_h seems to be implausible when considering the high flexibility of our plants that streamline with the flow at higher wind velocities. However, this can be explained by the fluttering motion of the upper part of the plants and the rather non-flexible stems of the lower part of the plants (see Appendix for discussion).

Finally it needs to be shown how well the definition $\tau_S'' = a\tau_S'$ (Eq. 14) works when combined with Eq. 9 to predict the peak stress ratio according to:

$$\left(\frac{\tau_S''}{\tau}\right)^{1/2} = \left(\frac{a}{(1-\sigma\lambda)\,(1+\beta\lambda)}\right)^{1/2}. \tag{16}$$

Figure 11 contains the same dataset as Fig. 6 but now with the modified model of Raupach (Eq. 16) applied to our data. The modified model provides a fit to the data as well as the old model using the constant m parameter within the measurement range. For very low roughness densities ($\log(\lambda) < -2$) the modified model seems to overestimate the general trend of the literature data, however, only the cylinder data from Musick et al. (1996) are noticeably lower than the prediction, which is the case for the whole λ range. We attribute this to the method

they employed to determine the shear stress ratio, which has been done visually at the onset of particle erosion.

The modified model results in stress-ratio predictions >1 at very low roughness densities $\lambda < 0.005 (\log(\lambda) < -2.25)$, which implies that $\tau_S'' > \tau$ (Fig. 11). At first glance, this seems to be unphysical, since $\tau_S'' = \tau_S' = \tau$ has to hold for $\lambda = 0$. However, it was already discussed in Sect. 4.3 that τ_S'' may be larger than τ at very low roughness densities. Therefore, the low roughness densities need to be realized by decreasing the number of roughness elements per unit area rather than by decreasing the roughness element size, to maintain the strength of the deflection of the airflow around each obstacle constant. A single, relatively large roughness element of the size of a plant or a block as used in our experiments on a large unit ground area might thus result in a high peak shear stress $\tau_S'' > \tau$. At the same time, the few remaining roughness elements do not result in a strong increase in the total stress τ above the canopy compared to the smooth floor case. With these assumptions, it is physically plausible that $\left(\tau_S''/\tau\right)^{1/2} > 1$ for low λ, furthermore, $\left(\tau_S''/\tau\right)^{1/2} \to a^{1/2} = \left(\tau_S''/\tau_S'\right)^{1/2}$ as $\lambda \to 0$ since τ_S' is the same as the total stress τ in the smooth floor case.

The latter allows for estimating the parameter a for roughness elements by using solely a single element and a single surface shear-stress sensor. First, the sensor is placed in the centre of the wind tunnel to measure the total stress τ, which is the same as the surface averaged stress in the smooth floor case τ_S' assuming a horizontally homogenous boundary layer. Second, the roughness element is placed close to the shear-stress sensor, so that the sensor is in the speed-up zone at the position where the peak surface shear stress τ_S'' is present. To check if the position of τ_S'' is measured correctly, the roughness element can be moved slightly until the correct position of τ_S'' is found. Figure 2c, d shows the locations of the speed-up zones for our low density plant and block cases. This procedure has been tested and as a result, $a = 1.49$ has been determined for a single live plant slightly larger than those used for the canopy experiments. The slightly larger plant results in a stronger deflection of the airflow around and thus in higher wind velocities in the speed-up zones. This in turn results in a slightly larger τ_S'' and a value compared to the canopy measurements where $a = 1.37$ was found. Additionally, the limited spatial measurement resolution in the canopy case potentially results in a slight underestimation of τ_S'' and thus a. The a parameter has also been determined for a circular cylinder (diameter = 50 mm, height = 90 mm) where $a = 2.12$ and for a block (width × depth × height = $60 \times 60 \times 100\,\text{mm}^3$) where $a = 2.79$ was found. The peak-mean stress ratio a can thus be seen as a value that quantifies the strength of the flow deflection around a wall-mounted obstacle. Larger values of a imply a stronger flow deflection around the obstacle, which results in larger peak stress values τ_S''.

The performance of the modified model (Eq. 16) is at least equivalent to the original Raupach model (Fig. 12). Figure 12 is an analogue of Fig. 9, but now compares the original model (Eq. 11) with a Re_h- and λ-averaged constant m parameter for the plants ($m = 0.67$) and for the blocks ($m = 0.40$) determined after Eq. 10 (Fig. 8) against the new modified model (Eq. 16) using an average of the independently determined a parameters from Fig. 10 ($a = 1.37$ for the plants and $a = 1.86$ for the blocks). The essential benefit of using the a parameter, however, is its independence of λ and Re_h and the relatively simple experimental set-up needed to determine a for different types of roughness elements compared to the extensive set-up needed to determine m accurately. Further, the definition of a is more physically based and the relationship of τ_S'' on τ_S', as well as its independency of Re_h and λ, can be made plausible using simple fluid dynamical arguments.

A limitation of the results presented here for real erosive conditions needs to be mentioned: for natural vegetation canopies with sediment on a partially sheltered surface, spatial

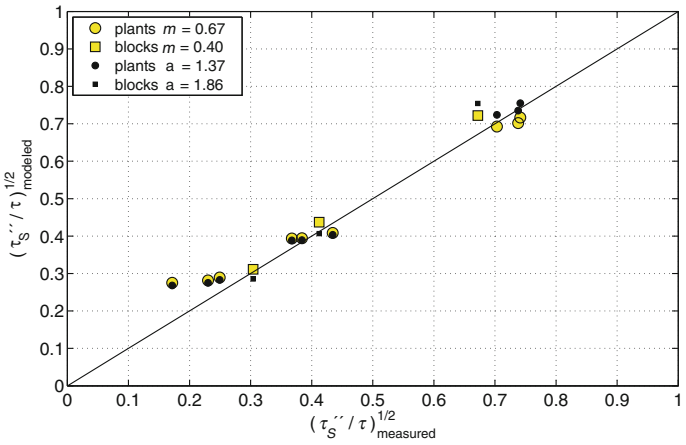

Fig. 12 Modelled measured peak surface shear-stress ratios $\left(\tau_S''/\tau\right)^{1/2}$ when using the original Raupach model with a constant m parameter and when using the new, modified model with the peak versus mean stress ratio a

gradients in the surface shear stress $\tau_S\,(x,\,y)$ result in horizontal particle transport that changes the surface topography (Raupach et al. 1993). According to this, the surface topography is reorganized so that the spatial gradients in $\tau_S\,(x,\,y)$ reduce and τ_S'' and τ_S' progressively adapt to each other. Raupach et al. (1993) concluded that the m parameter (and thus also the new a parameter) depends on the surface morphology and changes towards one as erosion reconfigures the surface. How strong m or a change towards one for natural vegetation canopies, however, depends on additional factors such as soil properties and the frequency of changes in the wind direction for example.

5 Conclusions and Outlook

Detailed investigations of the applicability and the accuracy of the model of Raupach (1992) and Raupach et al. (1993), which predicts the ratio of the surface shear stress τ_S to the total stress τ above vegetation canopies of different densities, are presented. It was found that the proportionality factor c (Eq. 7), which was formerly rather unspecified, can be set to $c = 0.27$ and that the model is capable of predicting the difference in total stress generation between our investigated block and plant canopies. Our plants, (*ryegrass*) ability to streamline with the flow results in a lower normalized total stress $\left(\tau/\rho U_h^2\right)^{1/2} = u_*/U_h$ generated by the plants than is generated by the rigid, non-porous blocks (Fig. 4b).

Although Raupach's model predicts the general differences in the average shear stress ratio $\left(\tau_S'/\tau\right)^{1/2}$ between the blocks and the plants adequately, the model does not capture the phenomenon that the blocks provide the lower stress ratios for the low roughness densities while our plant species used for the experiments provides the lower stress ratios for the high roughness densities (Fig. 5). Characteristics such as the porosity, the flexibility and the shape of the roughness elements can have complex influences on the stress partition and its dependency on λ. In the case of the peak stress ratio $\left(\tau_S''/\tau\right)^{1/2}$, the results for the blocks and the plants agree quite well because the blocks result in both a higher peak surface shear stress τ_S'' as well as total stress τ compared to the plants (Fig. 6). This result suggests that experiments

using plant imitations are capable of representing live plant canopies quite well with respect to investigations of $\left(\tau_S''/\tau\right)^{1/2}$.

Moreover, it was found that the empirical model parameter m, which relates the peak τ_S'' to the average τ_S' surface shear stress (Eq. 10), is impracticably defined in Raupach's model and that a new more physically-based definition in the form of $\tau_S'' = a\tau_S'$ (Eq. 14) results in model predictions of $\left(\tau_S''/\tau\right)^{1/2}$ that are as accurate as the original formulation. The main benefit of the new definition is that a is found to be independent of the roughness density λ for the plants and the freestream velocity U_δ, unlike m, which makes it easier of determining a than m. A method was suggested of determining a for various roughness elements by using a relatively simple experimental set-up.

Although our live plant canopies partly differ from natural vegetation canopies, the fact that our plants are of similar size, trimmed to a standard height and arranged with regular spacing allowed us to systematically investigate the influence of plant flexibility and porosity on the shear-stress partition. In addition, the live plant canopies used here are far closer to natural plant canopies than any roughness array used in previous wind-tunnel investigations of shear-stress partitioning and results may be similar for other plant species with comparable morphology.

Further improvements of the model may be accomplished by quantifying the increase in the horizontal coverage of the surface and the fluttering capability of flexible plants when increasing the wind velocities. The fluttering of the plants was found to result in a relatively large total stress for skimming flow regimes. Supplementary investigations may be performed to determine the parameters σ, β and a for a range of different plant species with variations in morphology, flexibility and porosity. Such a dataset can then be used by modellers and practitioners.

Acknowledgments We would like to thank the Swiss National Science Foundation (SNF) and the Vontobel foundation for financing this project. Thanks also to the SLF workshop and GS technology for supporting us with the development and the production of the measurement technique and the experimental set-up. Thanks also to Dr. Katherine Leonard, Dr. Andrew Clifton, Dr. Katrin Burri and Benjamin Eggert for their help with the wind-tunnel experiments and many fruitful discussions. Finally we would like to thank the reviewers for helping to improve the quality of the final manuscript.

Appendix: Re_h-Independency of a for Plants

In Sect. 4.4, it was shown that for our highly flexible plants (*rye grass*), the peak mean stress ratio a is independent of the free-stream velocity U_δ or the Reynolds number Re_h, respectively (Fig. 10). The strong linearity in $\tau_S''(U_\delta) = a\tau_S'(U_\delta)$ (Eq. 14) seems at first view to be implausible for flexible plant as for higher wind velocities, where the plant frontal area A_f and the drag coefficient C_R decrease (Fig. 3), a Re_h dependence of the surface shear stress τ_S and accordingly of a would be expected. However, there are substantive arguments that support the obtained linearity for the plants.

The spatio-temporally averaged wind velocity $\langle U_i \rangle$ inside the plant canopy increases with U_δ (see Sect. 4.4). The plant frontal area A_f decreases as the plants streamline with the flow (Fig. 13), which in turn results in an additional slight increase of $\langle U_i \rangle$ caused by the plant flexibility. Since now the local stress $\tau_S\,(x, y)$ scales with $\langle U_i \rangle^2$ (see Sect. 4.4), τ_S'' and τ_S' similarly increase with U_δ or $\langle U_i \rangle$ and $\tau_S'' = a\tau_S'$ holds also for flexible plants. In other words: when the plants streamline with the flow, resulting in slightly higher wind velocities close to the ground, both the peak as well as the mean surface shear stress increase similarly.

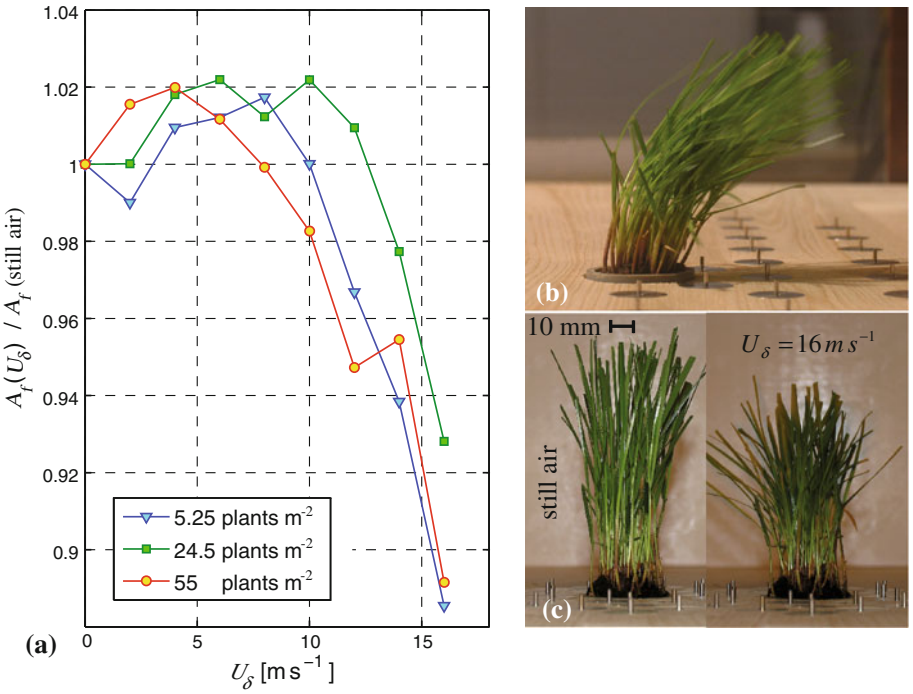

Fig. 13 **a** Temporally-averaged frontal area A_f of the plants normalized by their still-air frontal area as a function of the freestream velocity U_δ and different canopy densities. **b** Plant (*Lolium perenne*) streamlining with the flow (low density case, $\lambda = 0.015$, $U_\delta = 16\,\mathrm{m\,s^{-1}}$) and **c** front view pictures (streamwise direction) of a plant in still air and for $U_\delta = 16\,\mathrm{m\,s^{-1}}$ (high density case, $\lambda = 0.178$) taken from Walter et al. (2012b)

The above explanation is only true if the strength of the flow deflection around a plant remains constant at higher wind velocities, so that τ_S'' and τ_S' increase similarly with $\langle U_i \rangle$. For a flexible plant with a favourable aerodynamic shape at higher wind velocities, one would expect exactly the opposite. Namely, that the strength of the flow deflection decreases for higher wind velocities so that τ_S'' does not increase as strongly as τ_S' with $\langle U_i \rangle$. However, the lower parts of our plants, the stems that connect the grass swards with the ground, are relatively inflexible (Fig. 13b, c), which supports the finding of a velocity independent strength of the flow deflection around the plant close to the ground.

Furthermore, the flexible blades of the upper part of the plants allow the plants to respond to the turbulence in the flow. The flexible plants are very efficient in absorbing the momentum of strong eddies and transforming this energy into the potential energy of elastic deformation. This stored elastic energy is then released in time intervals of low turbulence and mean wind velocities, forcing the plant to re-erect to its still-air shape. As a result, the time-averaged frontal area A_f does not change much with flow velocity even for our highly flexible plants (Fig. 13a). First, A_f increases slightly by about 2 % for intermediate wind velocities (around $U_\delta = 8\,\mathrm{m\,s^{-1}}$) because the blades of the plants expand in the flow. Then, A_f decreases only by about 10 % when increasing U_δ from 8 to $16\,\mathrm{m\,s^{-1}}$ (Fig. 13). This small decrease in A_f suggests a rather small influence of the plant flexibility on the strength of the flow deflection for different wind velocities and additionally supports the finding that a is independent of

Re_h. The decrease in A_f of the plants appears to be the reason for the approximate 10 % reduction in the drag coefficient C_R at higher wind velocities (Fig. 3).

References

Arya SPS (1975) A drag partition theory for determining the large-scale roughness parameter and wind stress on the Arctic pack ice. J Geophys Res 80:3447–3454

Bagnold R (1941) The physics of blown sand and desert dunes. Meghuen, London 265 pp

Brown S, Nickling WG, Gillies JA (2008) A wind tunnel examination of shear stress partitioning for an assortment of surface roughness distributions. J Geophys Res. doi:10.1029/2007JF000790

Burri K, Gromke C, Graf F (2011a) Mycorrhizal fungi protect the soil from wind erosion: a wind tunnel study. Land Degrad Dev. doi:10.1002/ldr.1136

Burri K, Gromke C, Lehning M, Graf F (2011b) Aeolian sediment transport over vegetation canopies: a wind tunnel study with live plants. Aeolian Res 3:205–213

Clifton A, Lehning M (2008) Improvement and validation of a snow saltation model using wind tunnel measurements. Earth Surface Process Landf 33:2156–2173. doi:10.1002/Esp.1673

Clifton A, Ruedi JD, Lehning M (2006) Snow saltation threshold measurements in a drifting-snow wind tunnel. J Glaciol 52(179):585–596

Clifton A, Manes C, Ruedi JD, Guala M, Lehning M (2008) On shear-driven ventilation of snow. Boundary-Layer Meteorol 126:249–261

Crawley DM, Nickling WG (2003) Drag partition for regularly-arrayed rough surfaces. Boundary-Layer Meteorol 107:445–468

Gillies JA, Nickling WG, King J (2002) Drag coefficient and plant form response to wind speed in three plant species: burning Bush (Euonymus alatus), Colorado Blue Spruce (Picea pungens glauca.), and Fountain Grass (Pennisetum setaceum). J Geophys Res. doi:10.1029/2001JD001259

Gillies JA, Nickling WG, King J (2007) Shear stress partitioning in large patches of roughness in the atmospheric inertial sublayer. Boundary-Layer Meteorol 122:367–396

Gromke C, Ruck B (2008) Aerodynamic modelling of trees for small-scale wind tunnel studies. Forestry 81:243–258

Gromke C, Manes C, Walter B, Lehning M, Guala M (2011) Aerodynamic roughness length of fresh snow. Boundary-Layer Meteorol. doi:10.1007/s10546-011-9623-3

Guala M, Manes C, Clifton A, Lehning M (2008) On the saltation of fresh snow in a wind tunnel: profile characterization and single particle statistics. J Geophys Res Earth Surf 113:F03024

Irwin HPAH (1981) A simple omnidirectional sensor for wind-tunnel studies of pedestrian-level winds. J Wind Eng Ind Aerodyn 7:219–239

King J, Nickling WG, Gillies JA (2006) Aeolian shear stress ratio measurements within mesquite-dominated landscapes of the Chihuahuan Desert, New Mexico, USA. Geomorphology 82:229–244

Lyles L, Allison BE (1975) Wind erosion: uniformly spacing nonerodible elements eliminates effects of wind direction variability. J Soil Water Conserv 30:225–226

Marshall JK (1971) Drag measurements in roughness arrays of varying density and distribution. Agric Meteorol 8:269–292

Musick HB, Gillette DA (1990) Field evaluation of relationships between a vegetation structural parameter and sheltering against wind erosion. Land Deg Rehabil 2:87–94

Musick HB, Trujillo SM, Truman CR (1996) Wind-tunnel modelling of the influence of vegetation structure on saltation threshold. Earth Surf Process Landf 21:589–605

Raupach MR (1992) Drag and drag partition on rough surfaces. Boundary-Layer Meteorol 60:375–395

Raupach MR, Antonia RA, Rajagopalan S (1991) Rough-wall turbulent boundary layers. Appl Mech Rev 44:1–25

Raupach MR, Gillette DA, Leys JF (1993) The effect of roughness elements on wind erosion threshold. J Geophys Res 98:3023–3029

Schlichting H (1936) Experimental investigations of the problem of surface roughness. NASA technical memorandum 823, Washington, DC

Shao Y, Yang Y (2005) A scheme for drag partition over rough surfaces. Atmos Environ 39:7351–7361

Shao Y, Yang Y (2008) A theory for drag partition over rough surfaces. J Geophys Res 113:F02S05

Walter B, Gromke C, Lehning M (2009) The SLF boundary layer wind tunnel—an experimental facility for aerodynamical investigations of living plants. In: 2nd international conference on wind effects on trees, Freiburg, Germany

Walter B, Gromke C, Leonard K, Clifton A, Lehning M (2012a) Spatially resolved skin friction velocity measurements using Irwin sensors: a calibration and accuracy analysis. J Wind Eng Ind Aerodyn. doi:10.1016/j.jweia.2012.02.018

Walter B, Gromke C, Leonard K, Manes C, Lehning M (2012b) Spatio-temporal surface shear stress variability in live plant canopies and cube arrays. Boundary-Layer Meteorol. doi:10.1007/s10546-011-9690-5

Wolfe SA, Nickling WG (1996) Shear stress partitioning in sparsely vegetated desert canopies. Earth Surf Process Landf 21:607–619

Wooding RA, Bradley EF, Marshall JK (1973) Drag due to regular arrays of roughness elements of varying geometry. Boundary-Layer Meteorol 5:285–308

Wyatt VE, Nickling WG (1997) Drag and shear stress partitioning in sparse desert creosote communities. Can J Earth Sci 34:1486–1498